Degradation Pathways and Efficiencies of Acid Blue 1 by Photocatalytic Reaction with ZnO Nanopowder

Chiing-Chang Chen,*,†,‡ Huan-Jung Fan,§ and Jeng-Lyan Jan§

Department of General Education, National Taichung Nursing College, Taichung 403, Taiwan, ROC, and Department of Environmental Engineering, Hungkuang University, Taichung 433, Taiwan, ROC

Received: February 4, 2008; Revised Manuscript Received: April 20, 2008

The ZnO-mediated photocatalysis process has been successfully applied to degradation of Acid Blue 1 (AB1) dye pollutants. To obtain a better understanding, the mechanistic details of this ZnO-assisted photodegradation of the AB1 dye with low Watt UV irradiation, a large number of the photodegradation intermediates were separated, identified, and characterized by the HPLC−PDA−ESI−MS and GC−MS techniques. The degradation progresses through competitive reactions such as *N*-de-ethylation, destruction of the conjugated structure, hydroxylation on the benzene ring, hydroxylation on sulfonylated benzene ring, and substitution. The probable photodegradation pathways were proposed and discussed.

1. Introduction

Heterogeneous photocatalysis has emerged an important destructive technology leading to the total mineralization of most of the organic pollutants including organic dyes.[1,2] TiO_2 is the most commonly used effective photocatalyst for a wide range of organic chemical degradation.[3] ZnO is another semiconductor investigated in recent years, as a potential photocatalyst. In some cases, ZnO, has been more effective than TiO_2.[4] The biggest advantage of ZnO in comparison with TiO_2 is that it absorbs over a larger fraction of the UV spectrum and absorps more light quanta than TiO_2.[5] On the other hand, the photocorrosion of ZnO is complete at pH lower than 4. The formation of Zn^{2+} is attributed to the oxidation of ZnO by h^+_{vb}.[6]

ZnO is a representative of the metal oxide class, which is important to the study of electrochemistry and catalysis. Methods of preparation and long-term stabilization of ZnO colloidal solutions are already available in the literature.[7] More recently, nano-ZnO has received much attention due to its low cost of production, high photoactivity in several photochemical and photoelectron-chemical processes, and UV light response to band gap 3.2 eV. However, eliminating environmental pollution based on nano-ZnO has been well explored despite offering a potentially fertile area for research in environmental chemistry. The ZnO-mediated photocatalysis process has been successfully used to degrade organic pollutants in the past few decades.[8–13]

Triarylmethane dyes are used extensively in the textile industry on nylon, cotton, wool, and silk, as well as for coloring oils, fats, waxes, varnishes, and plastics. The paper, food, cosmetic, and leather industries are also major consumers of these dyes.[14] Additionally, they are applied as staining agents in bacteriological and histopathological processes. The photocytotoxicity of triarylmethane dyes based on reactive oxygen species production is tested intensively with regard to their photodynamic therapy.[15] Thyroid peroxidase-catalyzed oxidation of the triarylmethane class of dyes results in the formation of various *N*-dealkylated primary and secondary aromatic amines, which have structures similar to aromatic amine carcinogens.[16]

Studies on ZnO-mediated photodegradation of different kinds of dyes have been reported in the literature,[17,18] and most of them included kinetic and photodegradation efficiency. On the other hand, an extensive investigation into dye-sensitized photoelectrochemical (PEC) cells has recently begun.[19,20] However, less attention has been paid to the study of the degradation mechanism and more to the identification of major transient intermediates, which have been recognized as very important aspects of these processes recently, especially in view of their practical applications.

In earlier reports,[4c] only photodegradation of the triarylmethane dye, ethyl violet, a cationic dye, has been investigated under a ZnO-assisted photodegradation system. Only some of the photodegradation intermediates of these dyes have been separated and identified, and the detailed mechanisms are still not extensively understood. However, the photodegradation of AB1, an anionic triarylmethane dye, under ZnO-mediated processes has not been studied, and the intermediates have not been isolated or identified by the HPLC−ESI−MS or GC−MS technique.

In this research, a ZnO-assisted photocatalytic degradation study of the AB1 dye under UV 365 nm light irradiation is reported. This research focuses on the identification of the reaction intermediates and understanding of the mechanistic details of the photodegradation of AB1 dye under the ZnO/UV process. Comparing the mechanisms of this study with previous ones,[6] some other mechanism, i.e., hydroxylation, and substitution reactions were all observed. The reaction mechanism of ZnO/UV proposed in this research would be useful for future application of the technology to the decoloration of dyes using solar energy, dye-sensitized photoelectrochemical, and solid-state solar cells.

2. Experimental Section

2.1. Materials and Reagents. The ZnO nanoparticle was obtained by Aldrich (particle size, ca. 50−70 nm; BET area, ca. 15−25 $m^2\ g^{-1}$). P25 TiO_2 was from Degussa, having a surface area of ca. 55 $m^2\ g^{-1}$ and a measured size of the primary particles around 20−30 nm. Acid blue 1 (C.I. 42045) was

* Author to whom correspondence should be addressed. E-mail: ccchen@ntcnc.edu.tw. Fax: +886-4-2219-4990. Tel: +886-4-2219-6975.
† National Taichung Nursing College.
‡ Current Address: Department of Science Application and Dissemination, National Taichung University, Taichung 403, taiwan, ROC.
§ Hungkuang University.

10.1021/jp801027r CCC: $40.75
Published on Web 07/15/2008

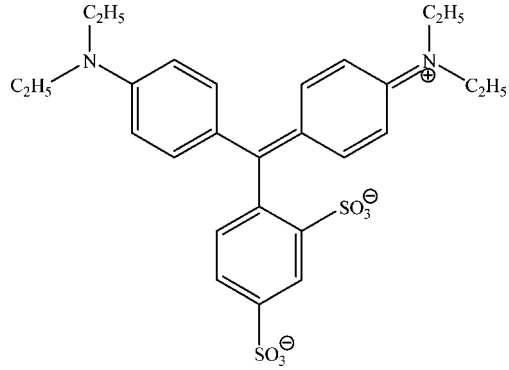

Figure 1. Chemical structure of AB1.

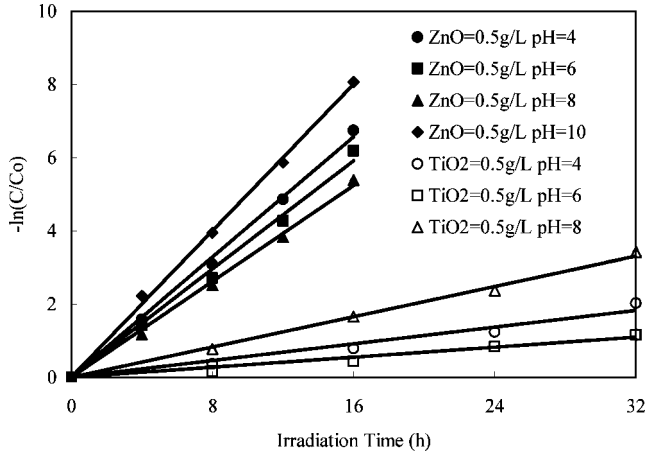

Figure 2. Photodegradation of AB1 in presence of ZnO and TiO_2 catalyst at different pH values. Catalyst: 0.5 g/L. AB1 concentration: 0.05 g/L.

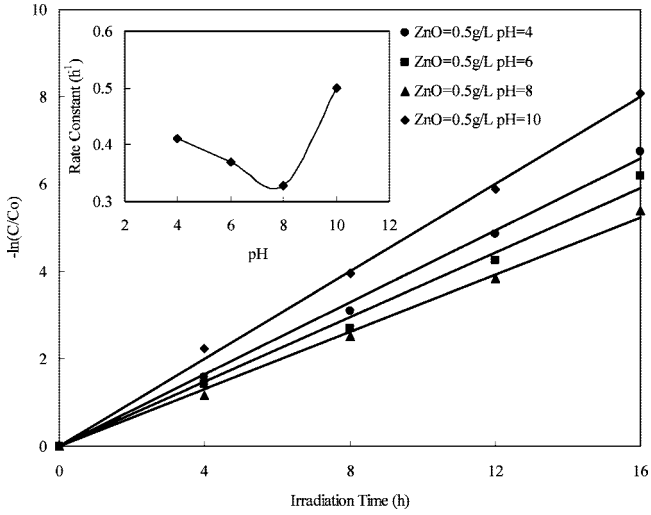

Figure 3. (a) pH effect on the AB1 photodegradation rate with concentrations of ZnO to be 0.5 g/L and AB1 to be 0.05 g/L. (b) The inset shows the first-order rate constants, *k*, as a function of pH.

provided by Tokyo Kasei Kogyo Co. and used as such without further purification. The chemical structure of AB1 is shown in Figure 1. The 4-(*N*,*N*-diethylamino)-4′-(*N*′,*N*′-diethylamino)benzophenone (DDBP) was obtained from Tokyo Kasei Kogyo Co. 4-Aminophenol (AP; analytical standard) was purchased from Riedel-de Haen. Reagent-grade ammonium acetate, nitric acid, sodium hydroxide, and HPLC-grade methanol were obtained from Merck.

2.2. Apparatus and Instruments. The C-75 Chromato-Vue Cabinet of UVP provides a wide area of illumination from the

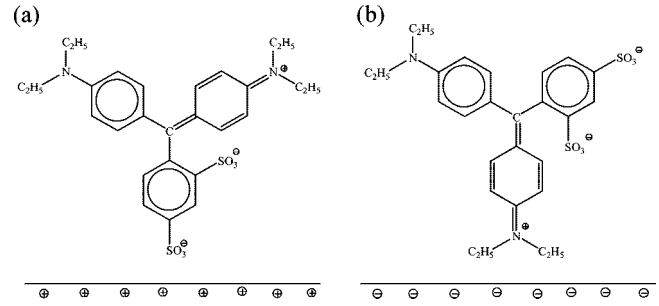

Figure 4. (a) Adsorption mode with a sulfonyl group and (b) adsorption mode with a diethylamino group.

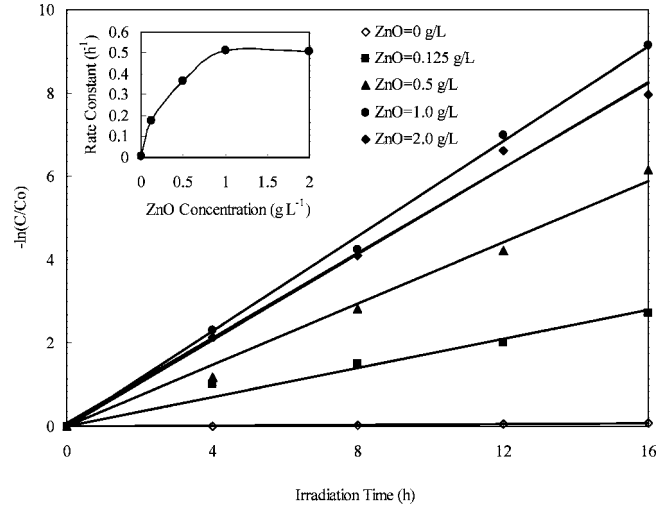

Figure 5. (a) Influence of the catalyst concentration on the photodegradation rate for the decomposition of AB1. (b) The inset shows the first-order rate constants, *k*, as a function of ZnO amount. Experimental condition: dye concentration (0.5 g/L), pH 4.

15-W 365 nm and UV tubes positioned on two sides of the cabinet interior.[21] The Waters ZQ LC/MS system, equipped with a binary pump, a photodiode array detector, an autosampler and a micromass detector, was used for separation and identification. The GC−MS system comes equipped with an AutoSystem XL Gas Chromatograph and a PerkinElmer TurboMass Gold Mass Spectrometer

2.3. Experimental Procedures. An aqueous TiO_2 dispersion was prepared by adding ZnO (or TiO_2) powder to a 100 mL solution containing the AB1 dye at appropriate concentrations. The reactor was supplied with 100 mL of dye solution and illuminated at 365 nm (using two 15 W lamps). For reaction in different pH media, the initial pH of the suspensions was adjusted by addition of either NaOH or HNO_3 solution. Prior to irradiation, the dispersions were magnetically stirred in the dark for ca. 30 min to ensure the establishment of the adsorption/desorption equilibrium. At any given irradiation time interval, the dispersion was continuously stirred, sampled (5 mL), centrifuged, and subsequently filtered through a Millipore filter (pore size, 0.22 μm) to separate the ZnO (or TiO_2) particles. Solutions are filtered after experiments then injected directly into the LC column.

2.4. Analytical Methods. ***2.4.1. HPLC−PDA−ESI−MS.*** After each irradiation cycle, the analysis of residence dye and organic intermediates were accomplished by HPLC−PDA−ESI−MS after the readjustment of the chromatographic conditions to make the mobile phase compatible with the working conditions of the mass spectrometer. LC was carried out on an Atlantis dC18 column (250 mm × 4.6 mm i.d., dp = 5 μm). Two different

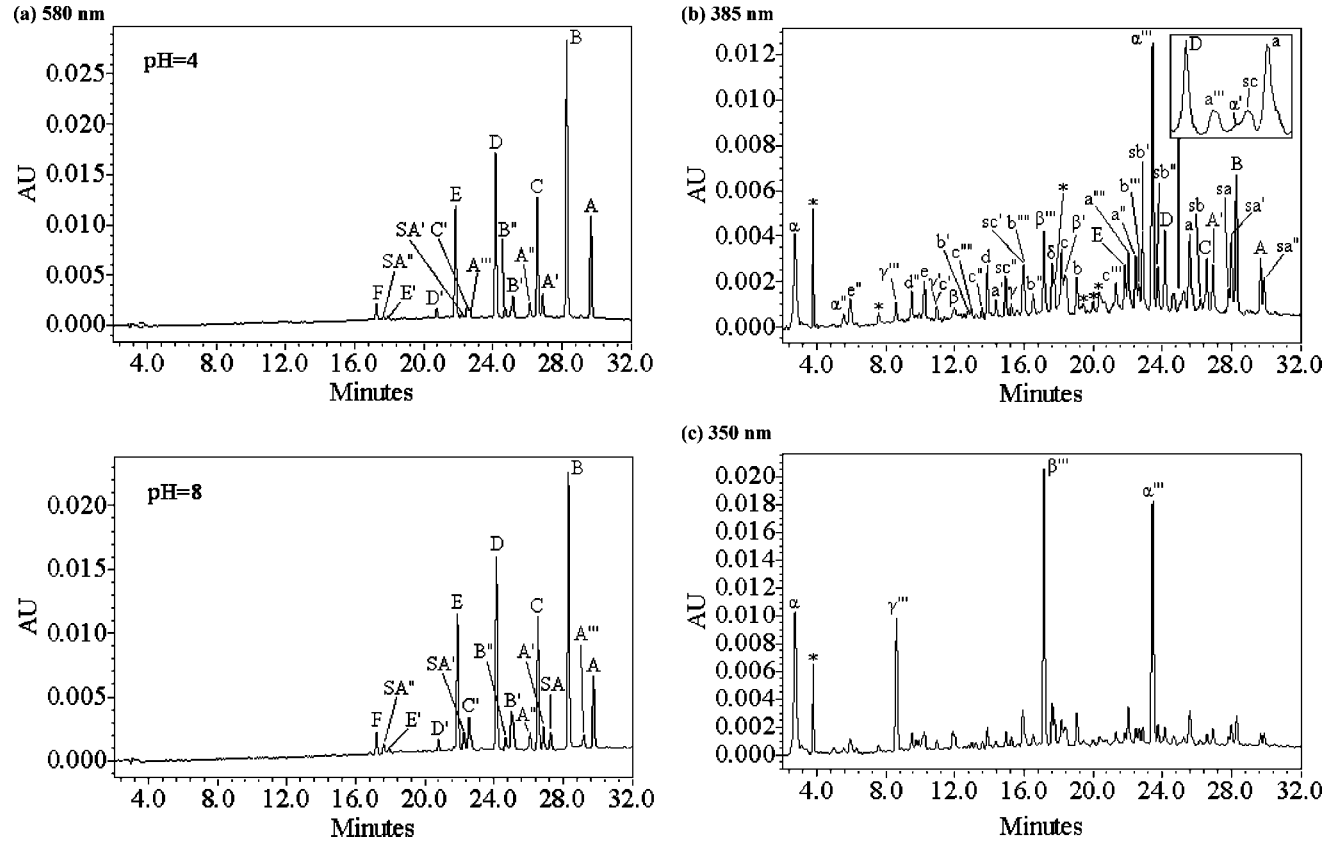

Figure 6. HPLC chromatogram of the photodecomposed intermediates with 16 h of irradiation, recorded at (a) 580 nm, pH 4 and 8, (b) 385 nm, pH 4, and (c) 350 nm, pH 4.

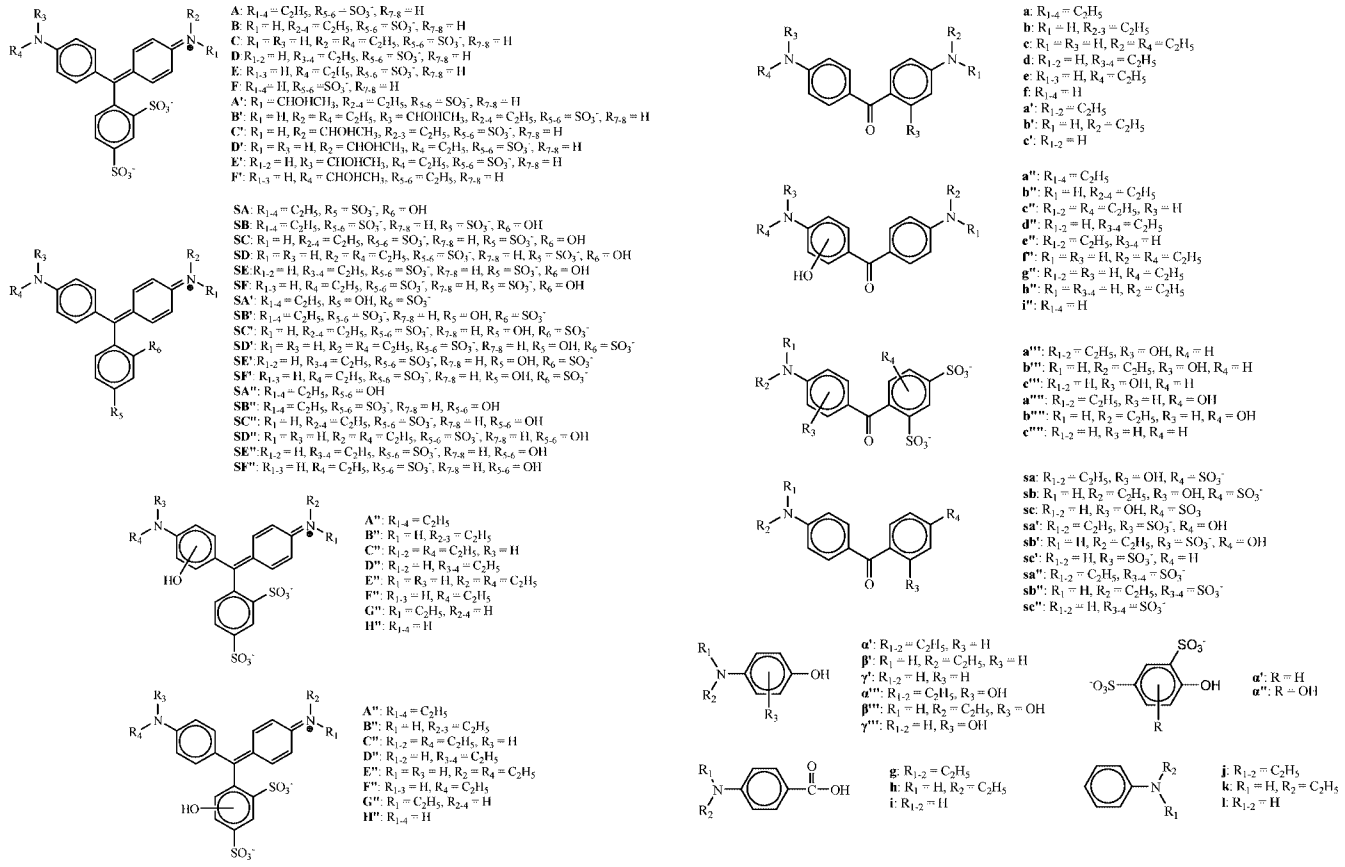

Figure 7. Chemical structure of photodecomposed intermediates.

kinds of solvents were prepared in this study. Solvent A was 25 mM aqueous ammonium acetate buffer (pH 6.9), and solvent B was methanol. The flow rate of the mobile phase was set at 1.0 mL/min. One linear gradient progressed from 95% A to

TABLE 1: Identification of the Intermediates of the Photodecomposed AB1 dye by HPLC−PDA−ESI−MS and GC−MS

intermediates	retention time (min)	$[M + H^+]/[MH^+]$ $(m/z)^a$	characteristic absorption (nm)
A	29.699	545.11/543.10	637.1, 412.6, 313.1
B	28.296	517.10/515.09	622.4, 403.0, 310.7
C	26.585	489.03/487.28	607.7, 395.7, 305.9
D	24.164	489.09/487.21	607.7, 369.9, 302.4
E	21.832	461.02/459.20	591.8, 388.5, 302.4
F	17.279	433.48/430.99	577.1, 384.8, 286.9
A′	26.892	561.10/559.15	647.0, 412.6, 313.1
B′	25.178	533.27/531.14	627.3, 413.8, 309.5
C′	22.521	533.19/531.00	640.8, 388.5, 305.9
D′	20.749	505.05/503.96	627.3, 304.7
E′	17.948	505.18/503.96	615.1, 302.4
A″	26.153	561.22/559.00	637.1, 411.4, 310.7
B″	24.722	533.15/531.34	623.6, 389.7, 317.9
A‴	22.708	561.13/559.39	638.4, 315.5
SA	28.103	481.54/479.52	621.2, 401.7, 310.7
SA′	22.223	481.22/479.26	611.4, 393.3, 308.3
SA″	17.682	481.44/479.21	607.7, 311.9
a	25.579	325.41	399.3, 289.2
b	18.365	297.32	395.7, 285.7
c	18.178	269.33	396.9, 280.9
d	13.867	269.25	388.5, 282.1
e	10.224	241.27	388.5, 273.8
a′	14.366	414.20/412.01	404.2, 284.5
b′	12.768	386.38/384.27	375.2, 283.3
c′	10.945	358/.51356.17	351.4, 283.8
a″	22.476	341.16/339.41	403.0, 271.4
b″	16.523	313.16/311.41	375.2, 273.8
c″	13.587	285.08/283.31	374.0, 272.6
d″	9.513	285.34/283.40	377.6, 273.8
e″	5.930	257.17/255.17	376.4, 272.6
a‴	24.647	430.27/428.24	435.6, 295.2
b‴	22.674	402.27/400.23	429.6, 297.6
c‴	21.322	374.17/372.38	413.8, 291.6
a⁗	22.032	430.14/428.05	369.1, 285.3
b⁗	15.972	402.27/400.17	369.1, 256.0
c⁗	12.962	374.29/372.28	366.7, 252.4
sa	27.831	350.08/348.51	436.9, 298.8
sb	26.237	322.03/320.20	436.9, 295.2
sc	25.231	294.18/292.26	428.4, 296.4
sa′	27.996	350.23/348.32	457.5, 275.0
sb′	22.882	322.33/320.16	419.9, 266.6
sc′	15.972	294.11/292.37	388.5, 256.0
sa″	29.897	286.22/284.57	412.6, 277.3
sb″	23.734	258.08/256.30	388.5, 273.8
sc″	14.932	230.18/228.41	388.5, 264.3
α	2.726	255.31/253.39	362.1
β	11.978	189.20	361.2
Γ	15.277	189.34	362.2
δ	17.635	123.01	362.1
α′	25.231	166.14	291.6
β′	18.365	138.08	288.1
γ′	10.945	110.13	285.7
α″	5.557	269.41	382.4
α‴	23.439	182.20	362.1
β‴	17.139	154.14	350.2
γ‴	8.572	126.07	332.2
j	30.56	149, 134,106, 77, 51[b]	N/A
k	28.59	121, 106, 77[b]	N/A
l	25.75	93, 66, 39[b]	N/A
m	23.43	59, 44, 43[b]	N/A
n	17.70	72, 55, 45, 27[b]	N/A
o	12.42	60, 45, 43[b]	N/A

[a] Positive- and Negative-Ion ESI Mass Numbers (m/z). [b] The intermediates (**j-o**) were identified by GC−MS and the other intermediates were identified by HPLC−PDA−ESI−MS.

50% A in 20 min and remained unchanged for 15 min; then another linear gradient progressed from 50% A to 10% A in 15 min and remained unchanged for 5 min; then another linear gradient progressed from 10% A to 95% A in 5 min. The column effluent was introduced into the ESI source of the mass spectrometer. Tube lens and capillary voltages were optimized for the maximum response during perfusion of the AB1 standard.

2.4.2. Gas Chromatography−Mass Spectrometry. For the identification of the reaction intermediates the solid-phase extraction method was applied to the samples prior to GC−MS analysis using Oasis HLB (hydrophilic/lipophilic balance). GC−MS analyses were performed on a Perkin-Elmer Auto-System-XL gas chromatograph interfaced to a TurboMass selective mass detector. Separation of the intermediates was carried out in a DB-5 capillary column, 60 m, 0.25 mm i.d., and 1.0 μm thick film. A split-splitless injector was used under the following conditions: injection volume 1 μL, injector temperature 280 °C, split flow 10 mL/min. Helium was used as carrier gas at a flow of 1 mL/min. The oven temperature program was 4.0 min at 40 °C, 4 °C/min to 80 °C (2 min), and 8 °C/min to 280 °C (9 min). The ion source and inlet line temperatures were set at 220 and 280 °C, respectively. The MS operated in electron ionization mode with a 70 eV, and the spectra were obtained at a scan range from m/z 35 to 300.

3. Results and Discussion

3.1. Catalyst Type. To compare the efficiencies of the catalyst we have carried out the photodegradation of AB1 with ZnO and TiO_2. As seen from Figure 2, nano-ZnO is a superior catalyst. The results showed that nano-ZnO exhibits higher photocatalytic activity than nano-TiO_2 at different pH values, the same trend was also obtained in other studies with ethyl violet.[6] Hence, all further studies were carried out using Aldrich nano-ZnO catalysts.

3.2. Control Experiments. Figure 1S (in Supporting Information) presents typical data showing the effect of photocatalyst. The experiment with ZnO only showed that a small amount of AB1 (about 0.3%) was adsorbed on the ZnO surface after 20 h. Control experiments performed in the dark indicated the hydrolysis and adsorption of AB1 on ZnO particles did not affect its concentration during these experiments. Next, the results of the photolysis and photocatalytic experiments showed that the photolysis reaction resulted in a 6.5% decrease in the AB1 concentration after 20 h whereas the AB1 was near 100% removed after 20 h in the case of the photocatalytic reaction. Therefore, we tentatively propose that AB1 photocatalytic degradation proceed by ZnO under UV irradiation.

3.3. Effect of pH. The zero point charge for ZnO is 9.0.[22] The role of pH on the photodegradation was studied in the pH range 4−10 at 50 mg/L dye concentration and 0.5 g/L catalyst loading. In early reports,[23] the photocatalytic degradation of the solute follows pseudo-first-order kinetics. By applying the following simple rate law, $-\ln(C/C_o) = kt$, to results of the current study, one can observe a linear relationship between $-\ln(C/C_o)$ and time (t), which is consistent with first-order kinetics. The slope k of the best-fit line through the data points represents the first-order rate constants for the corresponding different pH value. The results (Figure 3) show that the rate of decolorization decreases and then increases with increasing pH, the rate constant exhibiting a sudden increase and attaining a maximum value approximately at pH 10, as seen also in Figure 3 (inset). At higher pH values, no photocorrosion of ZnO takes place. A more efficient formation of the hydroxyl radical occurs in alkaline. AB1 has a diethylamino group in its structure, which is positively charged; therefore, dye may be absorbed onto the photocatalyst surface effectively. The formation of active $^{\bullet}OH$ species is favored with higher pH values, due to improved transfer of holes to the adsorbed hydroxyls. In a good agreement with the adsorption mechanism proposed by Chen et al.,[4c] our

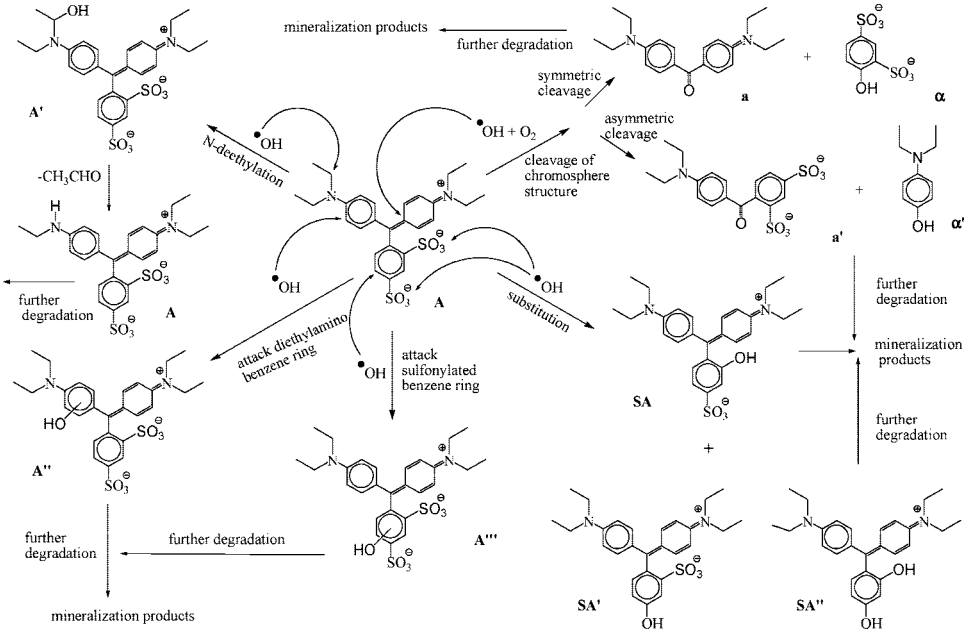

Figure 8. Proposed photodegradation mechanism of the AB1.

results indicate that the ZnO surface is negatively charged and that the AB1 was adsorbed onto the ZnO surface through the positive ammonium groups. Although the AB1 dye can be adsorbed onto the ZnO surface to some extent in alkaline media, when the pH value is too high, the dye molecules will change to a leuco compound.[23]

On the other hand, a noticeable increase in the photodegradation rate of the AB1 was observed when the pH had decreased to the 4−8 range. The photocorrosion of ZnO is complete at pH lower than 4. The formation of Zn^{2+} is attributed to the oxidation of ZnO by h^+_{vb}.[24,25] In addition, the anionic AB1 dye was found easily to adsorb onto the ZnO surface (positively charged) through the negative sulfonyl groups, and hence the photodegradation process of AB1 remained quick. The results show that the photodegradation rate at pH 4 was lower than that at pH 10, but higher than that at pH 6 and 8.

These results indicate that when the ZnO surface is negatively charged, the AB1 adsorbs onto it through the positive diethylamino groups. When the ZnO surface is positively charged, the AB1 adsorbs onto it through the negative sulfonyl groups (Figure 4). A similar effect of the pH on the adsorption and photocatalytic reaction has been reported for the degradation of sulforhodamine-B.[26]

3.4. Effect of Catalyst Concentration. The amount of photocatalyst is an important parameter that can affect the degradation rate of organic compounds in slurry photocatalytic processes. Hence, to investigate the relation between photocatalyst loading and rate constant k (h^{-1}), the amount of catalyst is varied between 0.1 and 2 g/L in a series of experiments under constant process conditions: dye concentration = 50 mg/L, pH = 6. Figure 5 shows first-order rate curves for various catalyst loadings. As expected, the reaction rate was found to increase and then decrease with the increase in the catalyst loading (Figure 5, inset). This is characteristic of heterogeneous photocatalysts, and the results are in agreement with earlier studies.[27] The photolysis reaction resulted in a decrease about 6.4% in the AB1 concentration after 16 h whereas, in the photocatalytic reaction, the AB1 was completely decomposed after 16 h. Above 1 g/L of ZnO, the initial rate of AB1 degradation was not affected further by a progressive increase in ZnO concentration. The maximal rate constant for AB1 appears at a ZnO concentration of around 1 g/L. This phenomenon may be due to the aggregation of ZnO particles at high concentrations causing a decrease in the number of surface active sites. It is known, however, that a practical limit of the scattering light (around 1 g/L) exists, above which the degradation rate will decrease due to the reduction of the photonic flux within the irradiated solution.[9]

3.5. UV−Visible Spectra. The depletion of the UV−visible spectra during the photodegradation process of the AB1 dye is illustrated in Figure 2S. In Figure 2S, the characteristic absorption band of the dye around 637.1 nm decreased rapidly, then a slight hypsochromic shift ($\Delta\lambda = 20.1$ nm and $\Delta\lambda = 15.9$ nm) appeared at pH 4 and 8, respectively. These results may indicate the photodegradation mechanism is favorable to cleavage of the whole conjugated chromophore structure of the AB1 dye. The result showed that the anionic dye AB1 was easily adsorbed on the positive ZnO surface by the sulfonyl group (Figure 4). Besides, in Figure 2S, the characteristic absorption band of the dye around 637.1 nm with a slight hypsochromic shift ($\Delta\lambda = 13.6$ nm) then decreased rapidly at pH 10, but no new absorption bands appeared, even in the ultraviolet range (200 nm < λ < 400 nm), indicating the possible formation of a series of *N*-de-ethylated intermediates, then cleavage of the whole conjugated chromophore structure of the AB1 dye, and/or degradation of the phenylic skeleton. Similar phenomena were also observed during the TiO_2-mediated photodegradation of malachite green.[21]

3.6. Separation and Identification of the Photodegradation Intermediates. Photocatalytic degradation of AB1 dye yielded a number of transient organic intermediates. Temporal variations occurring in the solution of the AB1 dye during the degradation process with UV irradiation were examined using HPLC coupled with a PDA detector and ESI mass spectrometry. The chromatograms at pH 4 are illustrated in Figure 6. The intermediates were identified, all with retention times of less than 32 min. We denoted the AB1 dye and its related intermediates as species **A-F**, **A′-E′**, **A″**, **A‴**, **SA**, **SA′**, **SA″**, **a-e**, **a′-c′**, **a″-e″**, **a‴-c‴**, **a⁗-c⁗**, **sa-sc**, **sa′-sc′**, **sa″-sc″**, **α**, **α′-γ′**, **α″** and **α‴-γ‴**. Except for the initial AB1 dye (peak **A**), the other peaks initially

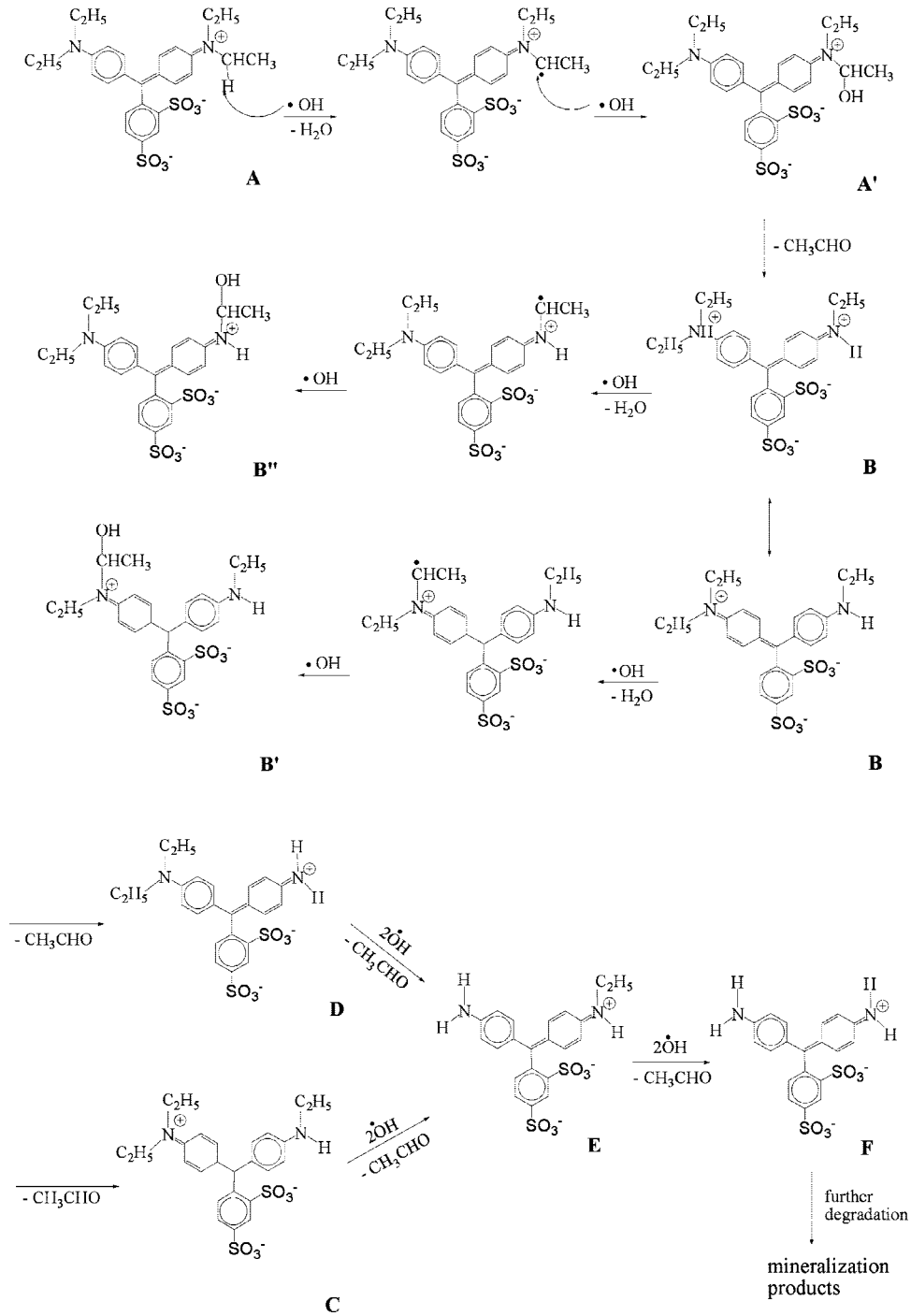

Figure 9. Proposed *N*-de-ethylation pathway of the AB1 dye.

increased before subsequently decreasing, indicating formation and transformation of the intermediates. The absorption bands showed that the whole conjugated chromophore structure of the AB1 dye, the benzophenone structure, and benzene structure might exist. The absorption spectra of each intermediate in the visible and ultraviolet spectral region are depicted in Figure 3S. The intermediates were further identified using the HPLC-ESI mass spectrometric method, and the relevant mass spectra are illustrated in Figure 4S. The molecular ion peaks appeared to be in the acid forms and/or basic forms of the intermediates. Results of HPLC chromatograms, UV−visible spectra, and HPLC-ESI mass spectra are summarized in Table 1. From the results of absorption and mass spectral analysis, they are identified as **A-F**, **A′-E′**, **A″**, **A‴**, **SA**, **SA′**, **SA″**, **a-e**, **a′-c′**, **a″-e″**, **a‴-c‴**, **a⁗-c⁗**, **sa-sc**, **sa′-sc′**, **sa″-sc″**, **α**, **α′-γ′**, **α″** and **α‴-γ‴** corresponding to the peaks **A-F**, **A′-E′**, **A″**, **A‴**, **SA**, **SA′**, **SA″**, **a-e**, **a′-c′**, **a″-e″**, **a‴-c‴**, **a⁗-c⁗**, **sa-sc**, **sa′-sc′**, **sa″-sc″**, **α**, **α′-γ′**, **α″** and **α‴-γ‴** in Figure 6, respectively. Several categories of intermediates can be distinguished in Figure 7 and Table 1. Additionally, the other peaks, designated with star marks, are depicted in Figure 6. The absorption bands from 450 to 200 nm are observed. The concentration of these intermediates may be too low to be examined by HPLC−ESI−MS. The partial intermediates identified in the study were also identified in our previous study using Michler's ethyl ketone and ethyl violet under TiO_2/UV processes.[28,29] The proposed intermediates (**a** and **γ′**) have been compared with standard material of 4-(*N*,*N*-

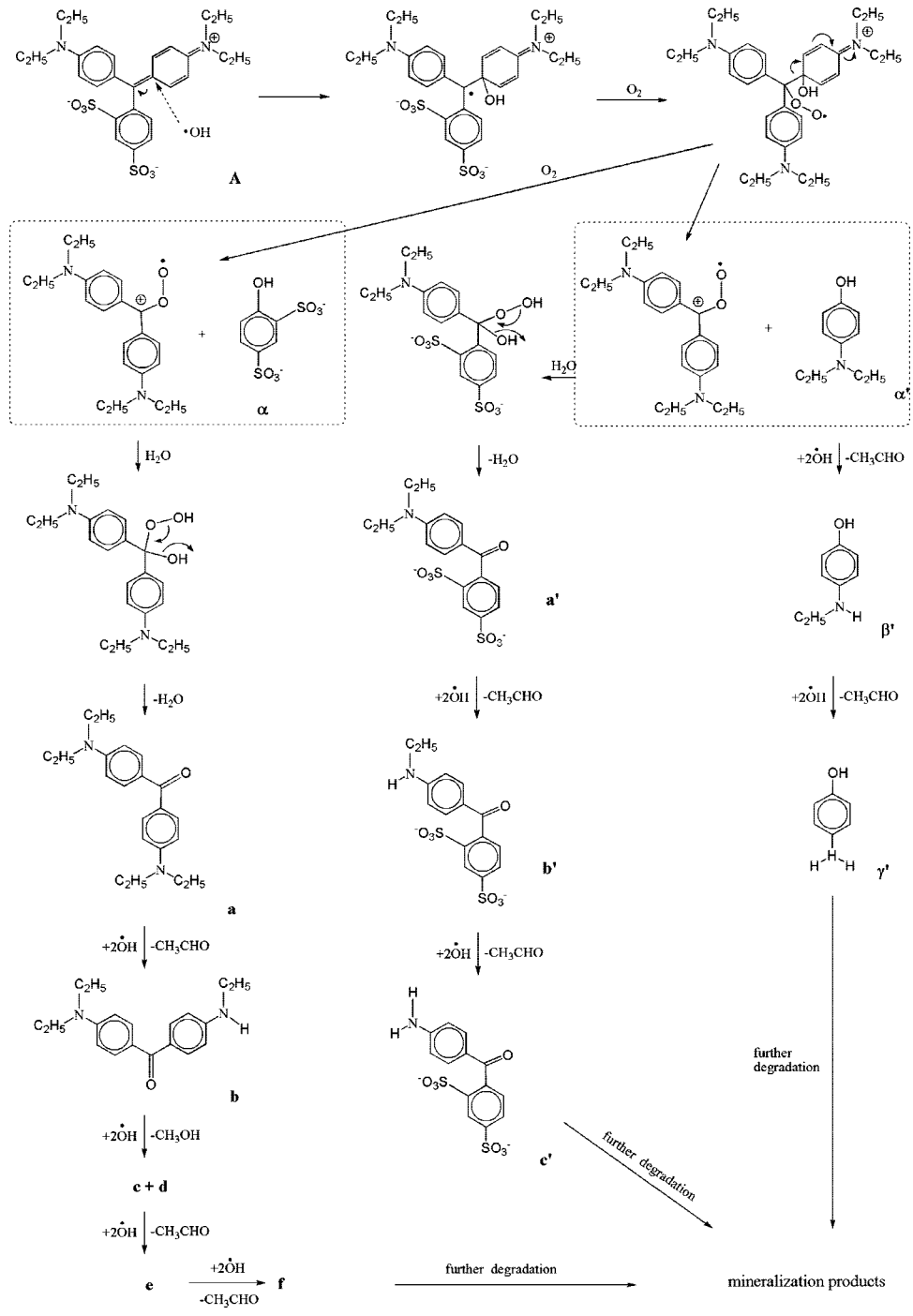

Figure 10. Proposed pathway of the cleavage of chromophore structure of the AB1.

diethylamino)-4′-(*N*′,*N*′-diethylamino)benzophenone and 4-aminobenzophenone. The retention time and absorption spectra are identical.

The other intermediates were marked in the GC−MS/EI chromatogram, and the relevant mass spectra are illustrated in Figure 5S. Table 1 presents the fragmentation patterns of the intermediates (**j-o**) and the corresponding compounds identified by interpretation of their MS spectra. The peaks eluting at 30.56, 28.59, 25.75, 23.43, 17.70, and 12.42 min during GC−MS were identified as *N*,*N*-diethylaminobenzene, *N*-ethylaminobenzene, aminobenzene, acetamide, 2-propenoic acid and acetic acid with fit values of 87%, 82%, 83%, 71%, 88%, and 95%, respectively, found by searching the mass spectra library. The intermediates identified in the study were also reported in a previous study of the MEK/TiO_2 system.[28] Further oxidation of organic substrates containing nitrogen to nitrate can be obtained by increasing the irradiation time.[30]

According to the number of the ethyl groups detached, we can characterize these intermediates. We found a pair of isomeric molecules, i.e., di-*N*-de-ethylated AB1 species, that differed only in their manner of loosening the ethyl groups from the benzyl groups. One of them, the **D** intermediate, was formed by the removal of an ethyl group from two different benzyl groups of the AB1 molecule. Loosening two methyl groups from the same benzyl group of the AB1 dye produced the other one, **C** intermediate. Therefore, considering the polarity of the **C** intermediates is greater than that of the **D** intermediate, we expected the latter to be eluted after the **C** intermediate. Also, to the extent that two *N*-ethyl groups are stronger auxochromic moieties than the *N*,*N*-diethyl or amino groups are, the maximal

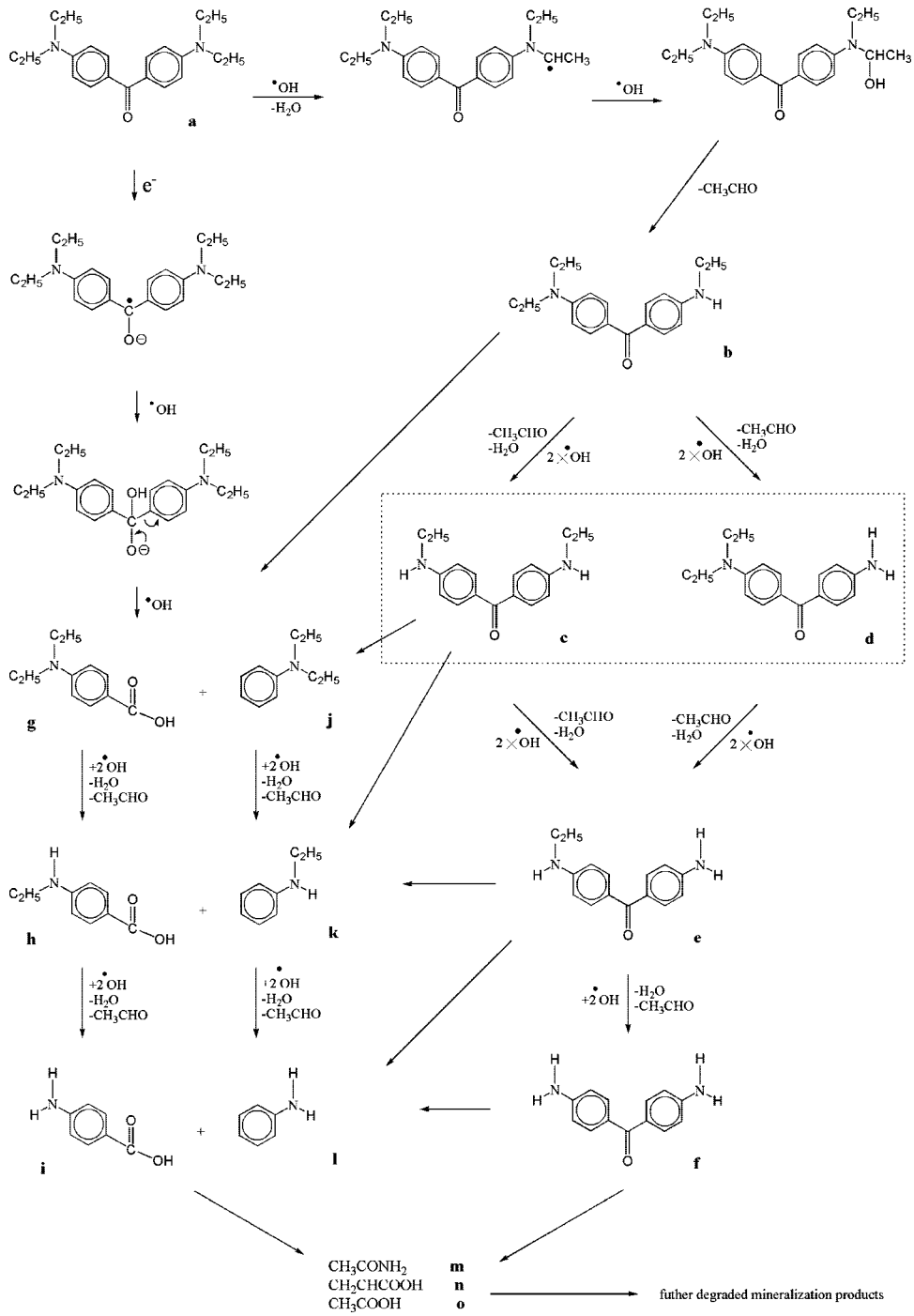

Figure 11. Proposed pathway of the destruction of the structure of the DDBP (**a**) derivatives by HPLC−MS and GC−MS.

absorption of the **C** intermediate was anticipated to occur at wavelengths shorter than the band position of the **D** intermediate. There is a similar situation in the other intermediates category.

A-**F** intermediates may be the *N*-de-ethylation of the **AB1** dye. **A′**-**E′** intermediates may be *N*-hydroxyethylated intermediates, the *N*-de-ethylated **AB1** species (Figure 9). The intermediates (**b**-**f**) may be the *N*-de-ethylation of **a**, produced by symmetric cleavage of the **AB1** chromophore ring structure (Figure 8). **b′**-**c′** and ***β′***-***γ′*** intermediates may be the *N*-de-ethylation of the **a′** and **α′**, produced by asymmetric cleavage of the **AB1** chromophore ring structure (Figure 10). **b**-**l** intermediates were presumed to result from the cleavage of **a** (Figure 11).[28] **A″**, **A‴**, **a**-**f**, **a″**-**f″**, **a‴**-**c‴**, **a⁗**-**c⁗**, **α**, **α′**-**γ′**, **α″**and **α‴**-**γ‴** intermediates were presumed to result from the formation of a series of the whole conjugated chromophore structure of the hydroxylated AB1 and their *N*-de-ethylation and cleavage of the **AB1** chromophore ring structure (Figure 12). Similar phenomena were also observed during the TiO_2-mediated photodegradation of Triazine and amaranth.[31,32] **SA**, **SA′**, **SA″**, **sa**-**sc**, **sa′**-**sc′**, **sa″**-**sc″**, ***β***-***δ***, and **α′**-**γ′** intermediates were presumed to result from the formation of a series of the whole conjugated chromophore structure of the substituted sulfonyl group of AB1 and their *N*-de-ethylation and cleavage of the **AB1** chromophore ring structure (Figure 13). In the TiO_2-mediated photodegradation of azo dyes[32,33] similar phenomena were observed.

3.7. Photodegradation Mechanisms of AB1. On the basis of all the above experimental results, we tentatively propose

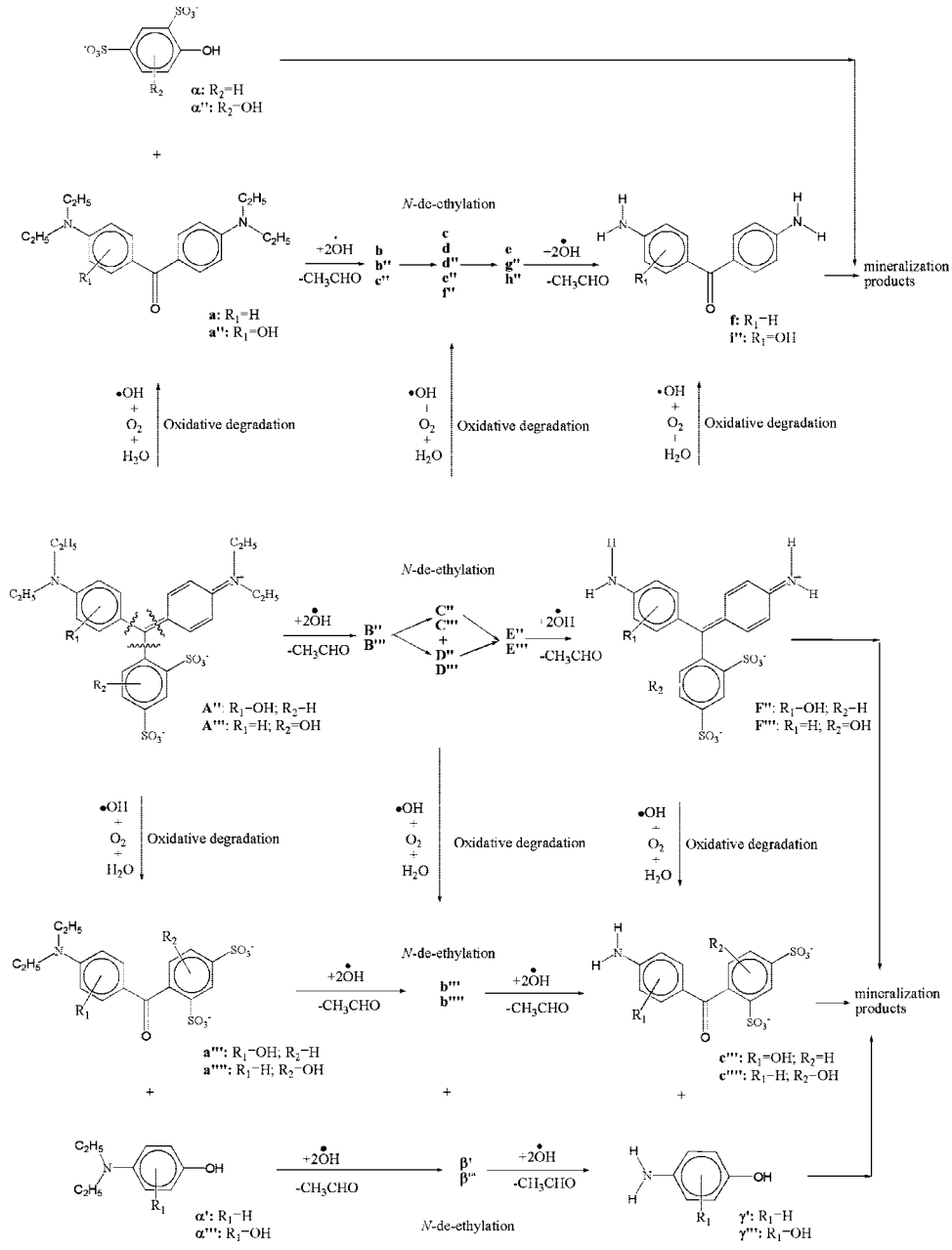

Figure 12. Proposed pathway of the degraded structure of the hydroxylated **AB1** derivatives (**A**″ and **A**‴).

the pathway of photodegradation depicted in Figure 8. In the Figure 9, the dye molecule in the AB1/ZnO system is adsorbed through the positively charged diethylamine function. Following the attraction of a hydrogen atom from the ethyl group of diethylamine by one •OH radical, and the attack by another •OH radical on the diethylamine radical and the formation of hydroxyethylated intermediates, the subsequent hydrolysis (or deprotonation) of intermediates yielded dehydroxyethylated intermediates, which were subsequently attacked by •OH radicals to lead ultimately to *N*-de-ethylation. The monode-ethylated dye, **B** intermediates, can also be adsorbed on the ZnO particle surface and be implicated in other similar events (•OH radical attraction and attack, hydrolysis, or deprotonation) to yield a bide-ethylated dye derivative, **C** and **D** intermediates. The *N*-de-ethylation process as described above continues until formation of the completely de-ethylated dye, **F** intermediates.

In Figure 10, the dye molecule in the AB1/ZnO system is adsorbed through the sulfonyl group of the AB1 chromophore structure. Following •OH radical attack the conjugated structure yields a carbon-centered radical, which is subsequently attacked by molecular oxygen to lead ultimately to **a**and **α** (or **a**′ and **α**′). The same process happened in the *N*-de-ethylated dye to produce the *N*-de-ethylated **a**and **α** (or **a**′and **α**′). The **a**and **α** (or **a**′and **α**′) can also be adsorbed on the ZnO particle surface and implicated in other similar events (•OH radical attraction and attack, hydrolysis or deprotonation, and/or oxygen attack) to yield a mono-*N*-de-ethylated derivative, **b** and ***β*** (or **b**′and ***β***′). Moreover, the same process happened in **c** to produce **d**. The *N*-de-ethylation process as described above continues until formation of the completely *N*-de-ethylated **a** (**a**′), **f** (**f**′), and *N*-de-ethylated **α**′, ***γ***′. All the above *N*-de-ethylation processes produced a series of *N*-dehydroxyethylated intermediates by the hydroxylation on the *N*-ethyl group.

In Figure 11, upon the transfer of an electron, the DDBP (**a**) and its *N*-demethylated species can form the radical anion, which can undergo the addition of a hydroxyl radical and form the anionic species, which upon cleavage can lead to the formation

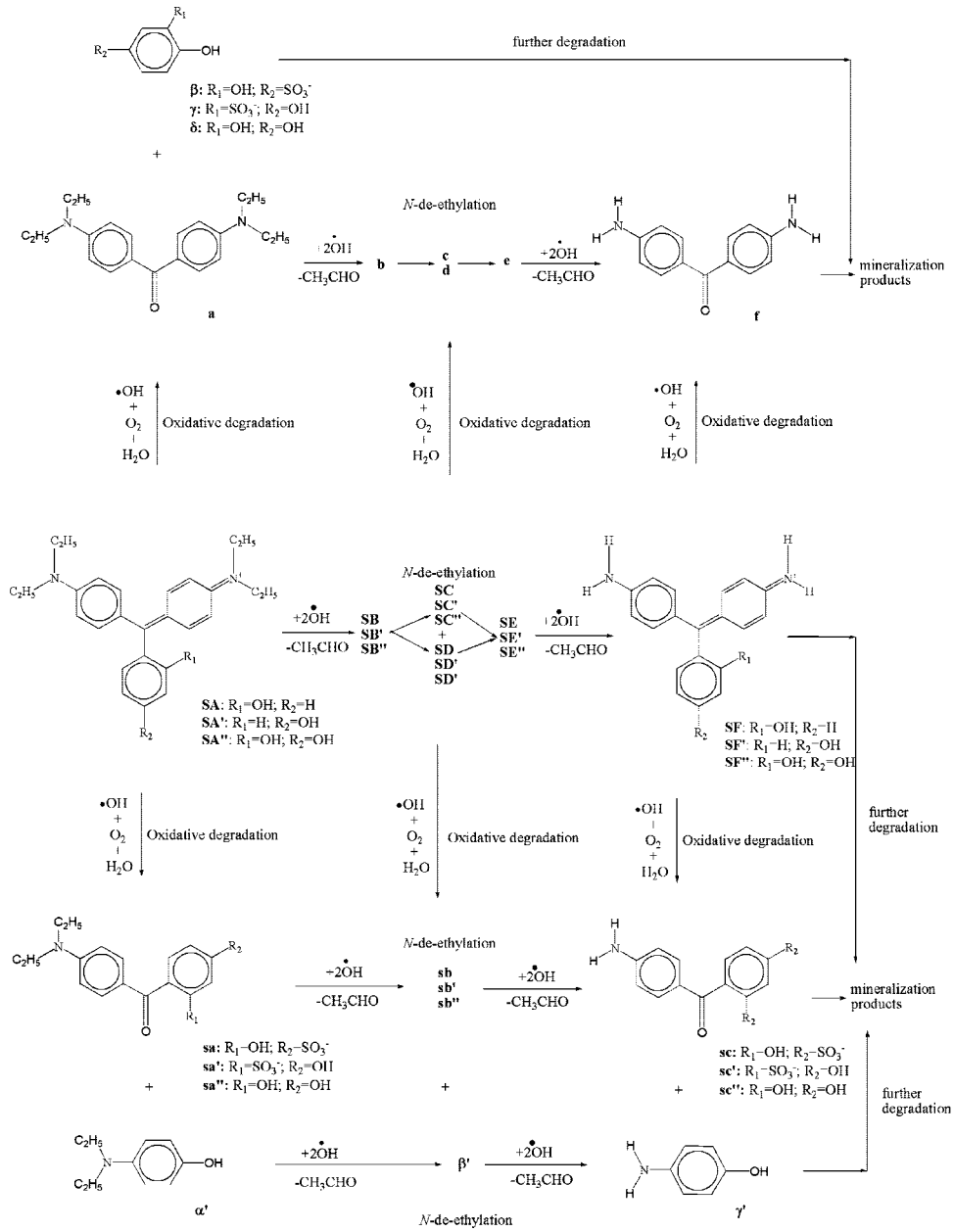

Figure 13. Proposed pathway of the degradation of the substituted **AB1** derivatives (**SA** and **SA′**).

of *N*-methylaminobenzene and aminobenzene. This is in agreement with mechanisms proposed by Muneer et al. for gentian violet.[34]

In Figure 12, the dye molecule in the AB1/ZnO system is adsorbed through the positively charged diethylamine function (or the negatively charged sulfonyl group). Following the attack on the (diethylamino)benzene (or disulfonylbenzene) ring of the AB1 chromophore structure by one •OH radical, the hydroxy-AB1 intermediate is formed. This then yields *N*-de-ethylation of intermediates (as in Figure 9) and/or cleavage of the chromophore structure (as in Figure 10) by •OH radicals to lead ultimately to intermediates.

In Figure 13, the dye molecule in the AB1/ZnO system is adsorbed through the negatively charged sulfonyl group of the AB1 chromophore structure. Subsequently, one (or two) •OH radical substitutes for the sulfonyl group and forms desulfonyl-hydroxy-AB1 intermediate. Then, this intermediate yields *N*-de-ethylation of intermediates (similar Figure 9) and/or cleavage of chromophore structure (similar Figure 10) by •OH radicals to lead ultimately to intermediates. All the intermediates were further degraded to produce CO_3^{2-}, CO_2, and NO_3^-.[30]

According to earlier reports,[6,23,35,36] most oxidative *N*-dealkylation processes (pathway I) are preceded by the formation of a nitrogen-centered radical and destruction of dye chromophore structures (pathway II) is preceded by the generation of a carbon-centered radical. •OH radical attacked the diethylaminobenzene (or disulfonylbenzene) ring of the AB1 chromophore structure (pathway III−IV) and substituted the sulfonyl group (pathway V) intermediates, which were found for the first time in ZnO-mediated photocatalysis process. Consistent with these, degradation of AB1 must occur via the five different photodegradation pathways listed in Figure 8.

Supporting Information Available: UV−visible spectra changes, absorption spectra of the photodegraded intermediates, and mass spectra of partial intermediates are available free of charge via the Internet at http://pubs.acs.org.

References and Notes

(1) Linsebigler, A. L.; Lu, G. Q.; Yates, J. T. *Chem. Rev.* **1995**, *95*, 735–758.

(2) Duxbury, D. F. *Chem. Rev.* **1993**, *93*, 381–433.

(3) Hoffman, M. R.; Martin, S. T.; Choi, W.; Bahnemann, W. *Chem. Rev.* **1995**, *95*, 69–96.

(4) (a) Kandavelu, V.; Kastien, H.; Thampi, K. R. *Appl. Catal. B: Environ.* **2004**, *48*, 101–111. (b) Wu, C. H. *Chemosphere* **2004**, *57*, 601–608. (c) Chen, C. C. *J. Mol. Catal. A: Chem.* **2007**, *264*, 82–92.

(5) (a) Bahnemann, D. W.; Kormann, C.; Hoffmann, M. R. *J. Phys. Chem.* **1987**, *91*, 3789–3798. (b) Sakthivel, S.; Neppolian, B.; Shankar, M. V.; Arabindoo, B.; Palanichamy, M.; Murugesan, V. *Sol. Energy Mater. Sol.* **2003**, *77*, 65–82.

(6) (a) Daneshvar, N.; Salari, D.; Khataee, A. R. *J. Photochem. Photobiol. A* **2004**, *162*, 317–322. (b) Spathis, P.; Poulios, I. *Corros. Sci.* **1995**, *37*, 673–680.

(7) Spanhel, L.; Anderson, M. A. *J. Am. Chem. Soc.* **1991**, *113*, 2826–2833.

(8) Evgenidou, E.; Konstantinou, I.; Fytianos, K.; Poulios, I.; Albanis, T. *Catal. Today* **2007**, *124*, 156–162.

(9) Pauporte, T.; Rathousky, J. *J. Phys. Chem. C.* **2007**, *111*, 7639–7644.

(10) Comparelli, R.; Fanizza, E.; Curri, M. L.; Cozzoli, P. D.; Mascolo, G.; Agostiano, A. *Appl. Catal. B: Environ.* **2005**, *60*, 1–11.

(11) Height, M. J.; Pratsinis, S. E.; Mekasuwandumrong, O.; Praserthdam, P. *Appl. Catal. B: Environ.* **2006**, *63*, 305–312.

(12) Sobana, N.; Swaminathan, M. *Sep. Purif. Technol.* **2007**, *56*, 101–107.

(13) Kamat, P. V.; Huehn, R.; Nicolaescu, R. *J. Phys. Chem. B* **2002**, *106*, 788–794.

(14) *Ullmann's Encyclopedia of Industrial Chemistry. Part A27. Triarylmethane and Diarylmethane Dyes*; 6th ed.; Wiley-VCH: New York, 2001.

(15) Baptista, M. S.; Indig, G. L. *J. Phys. Chem. B.* **1998**, *102*, 4678–4688.

(16) Cho, B. P.; Yang, T.; Blankenship, L. R.; Moody, J. D.; Churchwell, M.; Bebland, F. A.; Culp, S. J. *Chem. Res. Toxicol.* **2003**, *16*, 285–294.

(17) Akyol, A.; Yatmaz, H. C.; Bayramoglu, M. *Appl. Catal. B: Environ.* **2004**, *54*, 19–24.

(18) Wu, C. H. *Chemosphere* **2004**, *57*, 601–608.

(19) Westermark, K.; Rensmo, H.; Keis, H. S. K.; Hagfeldt, A.; Ojameauml, L.; Persson, P. *J. Phys. Chem. B* **2002**, *106*, 10102–10107.

(20) Bahadur, L.; Srivastava, P. *Sol. Energy Mater. Sol. Cells* **2003**, *79*, 235–248.

(21) Chen, C. C.; Lu, C. S.; Mai, F. D.; Weng, C. S. *J. Harad. Mat. B* **2006**, *137*, 1600–1607.

(22) Daneshvar, N.; Salari, D.; Khataee, A. R. *J. Photochem. Photobiol. A* **2004**, *162*, 317–322.

(23) Chen, C. C.; Lu, C. S. *Environ. Sci. Technol.* **2007**, *41*, 4389–4396.

(24) Evgenidou, E.; Fytianos, K.; Poulios, I. *Appl. Catal., B* **2005**, *59*, 81–89.

(25) Fernandez, J.; Kiwi, M.; Lizama, C.; Freer, J.; Baeza, J.; Mansilla, H. D. *J. Photochem. Photobiol. A* **2002**, *151*, 213–219.

(26) Liu, G.; Li, X.; Zhao, J.; Hidaka, H.; Serpone, N. *Environ. Sci. Technol.* **2000**, *34*, 3982–3990.

(27) Parra, S.; Stanca, S. E.; Guasaquillo, I.; Thampi, K. R. *Appl. Catal. B: Environ.* **2004**, *51*, 107–116.

(28) Lu, C. S.; Chen, C. C.; Mai, F. D.; Wu, Y. C. *J. Photochem. Photobiol. A: Chem.* **2007**, *187*, 167–176.

(29) Chen, C. C.; Lu, C. S.; Chung, Y. C. *J. Photochem. Photobiol. A: Chem.* **2006**, *181*, 120–125.

(30) Prevot, A. B.; Baiocchi, C.; Brussino, M. C.; Pramauro, E.; Savarino, P.; Augugliaro, V.; Marci, G.; Palmisano, L. *Environ. Sci. Technol.* **2001**, *35*, 971–976.

(31) Watanabe, N.; Horikoshi, S.; Kawasaki, A.; Hidaka, H.; Serpone, N. *Environ. Sci. Technol.* **2005**, *39*, 2320–2326.

(32) Karkmaz, M.; Puzenat, E.; Guillard, C.; Herrmann, J. M. *Appl. Catal. B: Environ.* **2004**, *51*, 183–194.

(33) Konstantinou, I. K.; Albanis, T. A. *Appl. Catal. B: Environ.* **2004**, *49*, 1–14.

(34) Saquib, M.; Muneer, M. *Dyes Pigments* **2003**, *56*, 37–49.

(35) Chen, C.; Lu, C. *J. Phys. Chem. C.* **2007**, *111*, 13922–13932.

(36) Zhao, J.; Wu, T.; Wu, K.; Oikawa, K.; Hidaka, H.; Serpone, N. *Environ. Sci. Technol.* **1998**, *32*, 2394–2400.

JP801027R